Proteins: Structure, Function, and Bioinformatics

WILEY

PROTEINS

RESEARCH ARTICLE

Structural Implications of HIV-1 Protease Subtype C Bound to Darunavir: A Molecular Dynamics Study

Sankaran Venkatachalam[1] | Sowmya Ramaswamy Krishnan[1] | Ramesh Pandian[2] | Yasien Sayed[2] | M. Michael Gromiha[1]

[1]Department of Biotechnology, Bhupat and Jyoti Mehta School of Biosciences, Indian Institute of Technology Madras, Chennai, India | [2]Protein Structure-Function Research Unit, School of Molecular and Cell Biology, University of the Witwatersrand, Johannesburg, South Africa

Correspondence: M. Michael Gromiha (gromiha@iitm.ac.in)

Received: 3 September 2024 | **Revised:** 8 November 2024 | **Accepted:** 18 February 2025

Funding: This work was supported by Department of Science and Technology, Government of India and South African National Research Foundation.

Keywords: AIDS | darunavir | DRV | HIV | MD simulations | protease | subtype C

ABSTRACT

In recent years, Human Immunodeficiency Virus (HIV) remains a significant global health challenge, with millions affected worldwide, particularly in Africa and sub-Saharan regions. Despite advances in antiretroviral therapies, the genetic variability of HIV, including different subtypes and drug-resistant strains, poses persistent obstacles in the development of universally effective treatments. This study focuses on the dynamics of HIV protease, a key enzyme in viral replication and maturation, particularly targeting subtype C and its double insertion (HL) variant L38HL, in the context of interaction with Darunavir (DRV), a second-generation nonpeptidic protease inhibitor approved by the FDA in 2006. Through molecular dynamics simulations, structural analyses, dynamic cross-correlation analyses, and binding energy calculations, we investigated differences in the binding of DRV to WT and L38HL HIV-1 protease. The findings highlight that the double insertion at the hinge induces variation in Φ and Ψ angles, leading to increased residue fluctuations, solvent-accessible surface area (SASA), and radius of gyration (R_g). This alters the overall structural compactness and the hydrophobic core crucial for drug binding. Subtle structural changes result in the loss of hydrogen bond interactions, reducing the binding energy of L38HL HIV-1 protease subtype C bound to DRV, leading to drug resistance.

1 | Introduction

Human Immunodeficiency Virus (HIV) is a viral pathogen that causes acquired immunodeficiency syndrome (AIDS), a condition that severely infects the human immune system [1, 2]. It is reported that approximately 3.6 billion people worldwide are infected with HIV [3]. Nevertheless, most of the infections happen among the African and sub-Saharan populations [4]. The first case of HIV was reported during the early 1980s, marking the beginning of a global health crisis [5]. Since then, its complex and diverse nature has challenged the efforts to combat the virus. HIV exhibits considerable genetic variability, resulting in the emergence of various subtypes. Among these, subtype B is prevalent across different regions [6].

Despite decades of research and advancements in treatment strategies, developing effective therapies against HIV remains challenging. One of the primary obstacles is the emergence of drug-resistant strains [7–9]. Consequently, current treatment approaches often rely on combination therapy, such as Highly Active Antiretroviral Therapy (HAART). HAART involves administering a combination of drugs targeting different stages of the HIV life cycle, including reverse transcriptase inhibitors, integrase inhibitors, and protease inhibitors [5, 10]. Among these therapeutic targets, HIV protease (PR) is crucial for viral replication and maturation [11]. HIV PR functions as a homodimer, with each monomer composed of 99 amino acids [12]. The enzyme's active site, crucial for proteolysis of viral polyproteins, is situated at the interface of the homodimer,

primarily constituted by Asp25/Asp25′. In addition to the active site, various structural elements within the enzyme, such as flaps, hinge, cantilever, and fulcrum (Figure 1) regulate the effective functioning of the enzyme [13]. Currently available FDA-approved protease inhibitors primarily target HIV protease subtype B [14, 15]. This limitation underscores the need for developing novel therapeutic agents that are specific to subtypes.

This study aims to understand the dynamics of HIV-1 protease subtype C and its insertion variant L38HL bound to Darunavir (DRV). HIV protease subtype B differs from subtype C by 8 distinct mutations [16]. Also, a recently identified insertion variant of subtype C, L38HL, characterized by two insertions at the 38th position [17], has been known to render the existing drugs ineffective [18, 19]. The 38th and 39th positions of the wild-type (WT) variant are L P, which upon insertion will change to L H L P. In total, the insertion variant exceeds the WT by 4 amino acids with two insertions at chains A and B each. The 3D structure of WT and L38HL is shown in Figure 1A,B.

In general, most of the FDA-approved drugs for the HIV-PR belong to the class of peptide-based inhibitors, i.e., they are designed based on the HIV PR substrate interactions. In contrast, DRV is a second-generation nonpeptidic protease inhibitor. The 2D chemical structure of DRV is shown in Figure 1C. It is an N,N-disubstituted benzenesulfonamide bearing an unsubstituted amino group at the 4th position. DRV was approved by the FDA for treating HIV in the year 2006 [20]. DRV bound to HIV PR is extensively studied using MD simulations and experiments. However, most of these works focus on the subtype B multidrug-resistant (MDR) variants [5]. A recent study on DRV bound to HIV PR subtype B from an MDR strain showed that the mutations increased the flap-tip flexibility due to the reduction of the flap–flap hydrophobic interactions [21]. While most of the existing studies are focused on HIV PR subtype B, this study focuses on understanding the mechanism of drug resistance in WT and the insertion variant of HIV protease subtype C bound to DRV using molecular dynamics simulations. We performed structural analyses, dynamic cross-correlation analyses, and binding energy calculations to explore the difference in the binding of DRV to WT and L38HL. Our findings emphasize that insertions at the hinge induced changes in Φ and Ψ angles, increasing residue fluctuations, solvent-accessible surface area (SASA), and radius of gyration (R_g). These alterations affect the overall structural compactness and the hydrophobic core essential for drug binding. Subtle structural modifications disrupt hydrogen bond interactions, thereby reducing the binding energy of L38HL bound to DRV, ultimately leading to drug resistance.

2 | Methods

2.1 | System Preparation

The 3D conformation of WT and L38HL bound to DRV was generated through homology modeling. The crystal structure of HIV protease subtype B bound to DRV (PDB ID 3SO9) was used as the template. The sequence corresponding to the WT was retrieved from (PDB ID 3U71), while information on the L38HL insertion was sourced from previous studies. The modeling was performed using MODELLER [22], and the protonation states were assigned using CHARMM-GUI [23]. The AMBER ff14SB force field [24] was employed to parameterize the proteins, and parameters for DRV were obtained using the general amber force field (GAFF2) [25]. Subsequently, both complexes were solvated in TIP3P water and neutralized by the addition of chloride counter-ions.

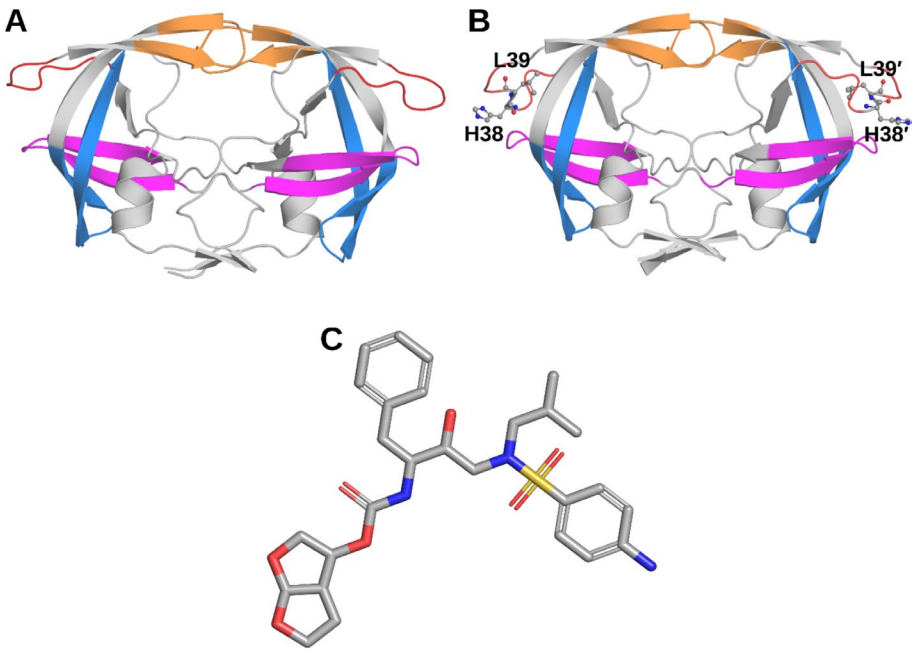

FIGURE 1 | Initial structure of HIV-1 protease subtype C in both its (A) WT and the (B) L38HL form. Functionally important regions including flap, cantilever, fulcrum, and hinge are highlighted in orange, blue, magenta, and red, respectively. The double amino acid insertion of residues (H and L) at the hinge region is represented in ball-and-sticks. (C) The 2D molecular structure of DRV.

2.2 | Molecular Dynamics Simulations

The solvated PR–DRV complexes were minimized using the SANDER module [26]. Initially, each system was relaxed with a harmonic restraint of 100 kcal·mol^{-1} Å^{-2}, followed by 6000 steps of minimization (3000 steps each of steepest descent and conjugate gradient). This was succeeded by a 4 ns equilibration period during which a positional restraint of 10 kcal·mol^{-1} Å^{-2} was applied to the PR–DRV complexes. Subsequently, an unrestrained production run was conducted for 300 ns with an integration time step of 2 fs, capturing a snapshot for every ps. Long-range electrostatics and van der Waals interactions were kept within a cut off of 12 Å, and long-range electrostatic interactions were managed using the particle mesh Ewald (PME) algorithm [27]. Additionally, the SHAKE algorithm [28] was utilized for treating hydrogen atoms. All the simulations were performed using the AMBER18 package [29]. To ensure reproducibility of the results, two independent simulations were performed for each of the WT and L38HL systems with varied initial velocities.

2.3 | Molecular Mechanics Generalized Born Surface Area

The binding free energy of DRV bound to WT and L38HL was calculated using MM/GBSA [30, 31]. The binding free energies were estimated using Equation (1).

$$\Delta G_{\text{bind}} = \Delta G_{\text{complex}} - \Delta G_{\text{receptor}} - \Delta G_{\text{ligand}} \tag{1}$$

where, ΔG_{bind} is the binding free energy, $\Delta G_{\text{complex}}$, $\Delta G_{\text{receptor}}$, ΔG_{ligand} are the free energies corresponding to PR–DRV complex, PR, and DRV, respectively. Further, each of the energy components in Equation (1) were calculated as mentioned in Equation (2)

$$\Delta G_{\text{bind}} = \Delta H - T\Delta S \tag{2}$$

where, ΔH corresponds to enthalpy of the system, and it is calculated as mentioned in Equation (3). $-T\Delta S$ corresponds to the entropy of the PR–DRV complexes, and it was calculated using Quasi-harmonic entropy approximation [32].

$$\Delta H = \Delta E_{\text{ele}} + \Delta E_{\text{vdW}} + \Delta G_{\text{GB}} + \Delta G_{\text{SA}} \tag{3}$$

where, ΔE_{ele}, ΔE_{vdW}, ΔG_{GB}, and ΔG_{SA} correspond to electrostatic, van der Waals, polar solvation and nonpolar solvation terms, respectively. The enthalpic contribution comes from two components; namely, the polar and the hydrophobic interactions. The polar interactions term is computed by the sum of electrostatic and polar solvation energies, and the hydrophobic interactions term is given by the sum of van der Waals interactions and nonpolar solvation free energy. 1000 snapshots extracted from the last 100 ns were used for MM/GBSA calculations.

2.4 | Dynamic Cross Correlation

The cross-correlation matrix (C_{ij}) corresponding to the Cα atoms of WT and L38HL was obtained using Equation (4).

$$C_{ij} = \frac{\langle \Delta r_i \cdot \Delta r_j \rangle}{\sqrt{\langle \Delta r_i^2 \rangle}\sqrt{\langle \Delta r_j^2 \rangle}} \tag{4}$$

where, r_i and r_j represent the displacement vectors from the mean position of the α carbons in the i^{th} and j^{th} residues, respectively. The angular brackets denote the time average over the simulation trajectory. The numerator captures the correlation given by the product of the coordinate shift vectors and the denominator corresponds to the normalization factor that limits the correlation, C_{ij} between −1 and +1 [33].

2.5 | Hydrogen Bond Analysis

The hydrogen bond analysis of the PR–DRV complexes was performed with a cut-off of donor–acceptor distance ≤3.5 Å and the donor-hydrogen–acceptor angle ≥135°. Hydrogen bonds between the PR and DRV having a frequency above 0.1 were obtained from each replica. Finally, the hydrogen bond frequencies corresponding to the average of the replicas were calculated. The residue pairs having an average hydrogen bond frequency of more than 10% were used for analyses.

2.6 | Trajectory Analysis

All the analyses, unless explicitly mentioned, were performed using the equilibrated trajectory (last 200 ns) with a snapshot frequency of 10 ps. The analyses presented in this work correspond to the average of two replicas, and they were performed using the CPPTRAJ module of AMBER Tools [26].

3 | Results

3.1 | Structural Stability and Changes due to Insertion From RMSD

To comprehensively assess the impact of insertions on the dynamics of the HIV PR backbone, the root-mean-squared deviation (RMSD) of Cα atoms relative to the initial conformation was computed (Figure 2). Figure 2A illustrates that both the WT and L38HL PR complexes reached equilibrium after approximately 50 and 100 ns, respectively. Notably, the L38HL PR complex displayed a noticeable transition until 100 ns, suggesting that the insertion may have prompted structural rearrangements. The mean RMSD values for the WT and L38HL PR complexes were 1.159 and 1.881 Å, respectively, with deviations ranging between ~0.6 and ~1.4 Å for the WT and ~0.7 and ~2.2 Å for L38HL.

Furthermore, to elucidate the structural modifications in L38HL (as indicated in the RMSD), representative structures corresponding to WT and L38HL obtained from the equilibrated region of the trajectory were superimposed (Figure 2B). The RMSD between the representative structures is ~0.7 Å. As seen from Figure 2B, the changes occur in the vicinity of the functionally important regions of PR; namely, the hinge and fulcrum. Furthermore, structural changes are also visible at the N- and C-terminal regions.

3.2 | Comparison of WT and L38HL Fluctuations at Residue Level

To understand the influence of the double insertion on structural flexibility, root-mean-squared fluctuation (RMSF) of backbone atoms in relation to their average coordinates was calculated. The purpose of this analysis was to characterize the impact of the L38HL mutation on the dynamic behavior of specific residues within the HIV PR structure. A comprehensive depiction of the RMSF profiles for residues of chains A and B, comparing the WT and L38HL PR complexes, is shown in Figure 3A,B. The overall trend in fluctuation observed for the L38HL closely resembles that of the WT. Notably, residues constituting the catalytic active site demonstrate stability, with RMSF values averaging around ~0.5 Å for both the WT and L38HL complexes. This suggests that the essential catalytic residues maintain consistent structural integrity despite the double insertion, emphasizing their crucial role in enzymatic function.

Conversely, residues within the hinge regions exhibit considerably higher levels of fluctuations, as indicated by higher RMSF values. The heightened fluctuations in the hinge regions align with the result from structural comparison (Figure 3B) depicting structural changes at the hinge due to double insertion. Specifically, residues

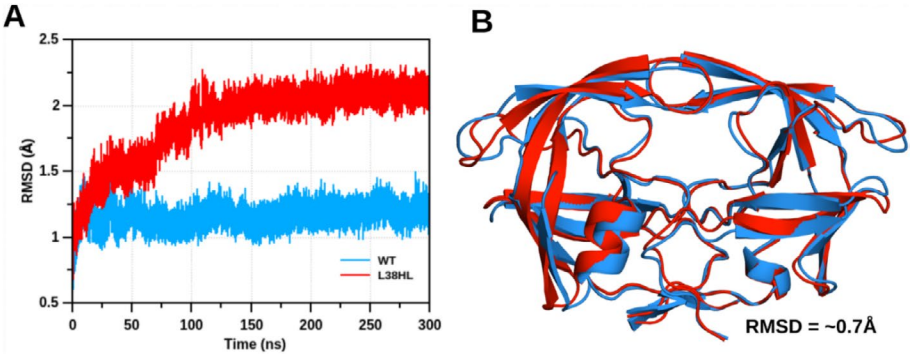

FIGURE 2 | (A) Average RMSD plotted for 300 ns simulation. (B) Superimposed structure of representative conformations from WT and L38HL depicting structural changes.

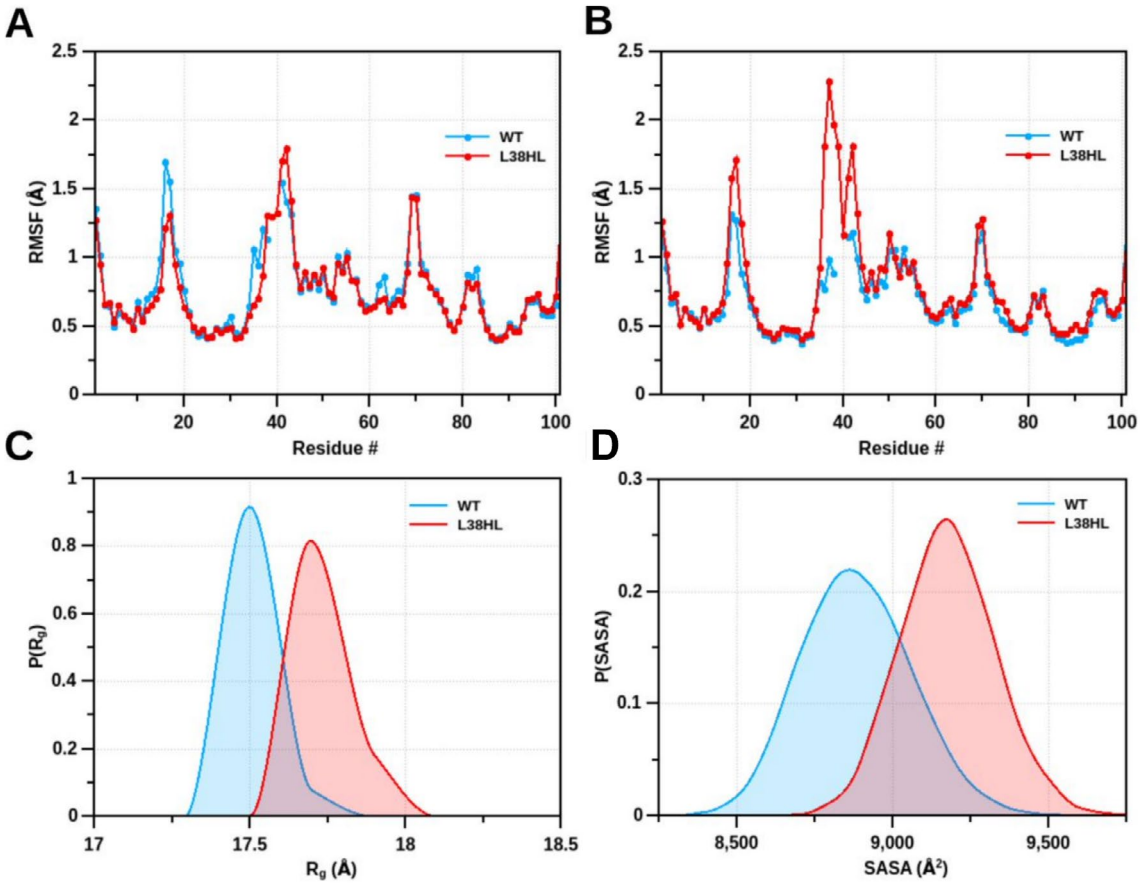

FIGURE 3 | Root-mean-square fluctuation analysis of (A) chain A and (B) chain B corresponding to WT and L38HL PR complexes. (C) Normalized histogram distribution of radius of gyration. (D) Normalized histogram distribution of solvent accessible surface area.

of both WT and L38HL from chain A exhibit higher fluctuations at the hinge. However, in chain B, the hinge residues corresponding to WT exhibit very lower fluctuations (~1.0 Å) whereas the hinge residues corresponding to L38HL exhibit much higher fluctuations (~2.3 Å). The double insertion at the chain B hinge may have triggered the fluctuation in this region, resulting in higher RMSF values compared to its WT counterpart. This implies that the double insertion mutation can have a potential localized impact on specific regions of the PR.

3.3 | Assessing the Changes in Compactness of WT and L38HL

To explore the impact of structural rearrangements on the spatial distribution of PR atoms around their axis, radius of gyration calculations were performed. The normalized histogram distribution of the WT and L38HL PR complexes is presented in Figure 3C. This analysis revealed that the WT exhibited relatively higher compactness compared to the L38HL PR complex, with a mean value of ~17.5 Å compared to ~17.8 Å observed for L38HL. The time evolution of the radius of gyration for the equilibrated trajectories is shown in SI Figure S1. Despite substantial RMSD deviations from the initial structure, the L38HL PR complex was found to maintain a compact nature, indicating that the structural rearrangements were localized and did not influence the overall compactness of the complex.

3.4 | Evaluating the Effect of Double Insertion on the Overall Shape of the PR

Subtle structural changes will significantly influence the function of an enzyme. Results from Sections 3.1 and 3.2 revealed significant structural perturbations due to the double insertion. Further, to unearth the overall changes in the shape of the enzyme, solvent accessible surface area (SASA) analysis was performed. The normalized histogram distribution of SASA is shown in Figure 3D, and the time evolution of SASA is given in SI Figure S2. The peak SASA value of the WT was ~8800 $Å^2$, whereas the L38HL had a major cluster of conformations at ~9200 $Å^2$. The wider curve for WT shows that most of the SASA values are between ~8500 and ~9200 $Å^2$. Interestingly, there is a significant overlap between the WT and L38HL distributions. Nevertheless, the shift in the peak for L38HL clearly suggests a change in the overall shape of the L38HL. This observed increment of ~400 $Å^2$ denotes a larger exposed surface area in the L38HL, which can be attributed to the double insertion. The increase in SASA in the L38HL structure can be due to heightened flexibility or modified interactions due to the insertion.

3.5 | Analyzing the Changes in Cross-Correlation Between WT and L38HL

The analysis of dynamic cross-correlation aims to elucidate correlation in the inter-atomic movements. Due to the complexity of simulations involving all atoms, the analysis is performed on only the Cα atoms, resulting in an $N \times N$ cross-correlation matrix, where N represents the total Cα atoms in the PR. In this study, the value of N is 198 and 202 for WT and L38HL, respectively. A heatmap of the cross-correlation matrix is shown in Figure 4. Continuous numbering of residues between the chains is followed for easy comparison. In WT (Figure 4A), residues from 1 to 99 belong to chain A, and residues from 100 to 198 belong to chain B. Similarly, in L38HL (Figure 4B) residues 1–101 correspond to chain A, and residues 102–202 correspond to chain B.

In Figure 4, region R1 depicts the cross-correlation between residues from the hinge to the binding site; R2 encompasses the cross-correlation between the hinge, binding site, and the

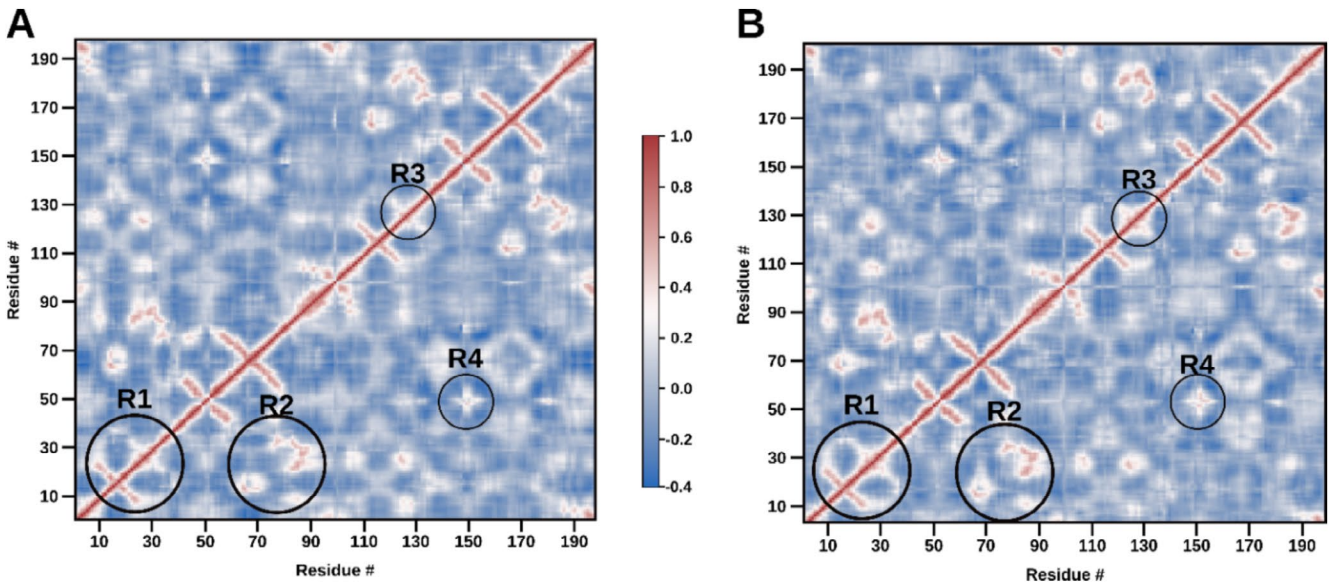

FIGURE 4 | Heatmap from dynamic cross-correlation analysis (A) WT (B) L38HL with continuous numbering (WT chain A: 1–99; WT chain B: 100–198; L38HL chain A: 1–101; L38HL chain B: 102–202). R1—residues encompassing the hinge to the binding site, R2—residues from the hinge, binding site, and C-terminal, R3—chain A –chain B hinge, R4—chain A–chain B flap. The scale of the heatmap is set based on the minimum value observed (−0.4) in terms of negative correlation.

C-terminal regions of chain A. Further, regions R3 and R4 correspond to chain A–chain B hinge and chain A–chain B flap. In the WT, region R1 exhibits a negative correlation, which is lost in L38HL, suggesting that the fluctuations are no longer correlated. Further, the residues near the protease's active site show a slight decrease in positive correlation in the L38HL as compared to the WT. On the other hand, region R2 in L38HL shows a slight increase in positive and a slight decrease in negative correlations. Additionally, in L38HL, a positive correlation is observed at the flap interface (R4). This illustrates that the fluctuations of the flap residues are in the same direction. Furthermore, a loss in the negative correlation is observed between chain A–chain B hinge residues. In essence, the insertion of residues at the hinge has triggered structural perturbations, which in turn may alter inter- and intra-molecular interactions owing to drug resistance in L38HL.

3.6 | Evaluating the Hydrogen Bond Interactions Between WT/L38HL PR and DRV

Hydrogen bond interactions are critical for governing the dynamics of the protein structure. Moreover, in the case of protein–ligand complexes, they are instrumental in determining the affinity of the ligand towards the target protein. Thus, the hydrogen bond interactions between WT/L38HL and DRV were computed (as described in Section 2.5) from the simulation trajectory. The average frequency of key atom pairs involved in hydrogen bonding corresponding to WT and L38HL is given in Tables 1 and 2, respectively, and a representative snapshot depicting the hydrogen bond interactions is shown in Figure 5. The O18 atom of DRV, in both WT and L38HL, is hydrogen bonded with the catalytic residues Asp25 and Asp25′ throughout the entire equilibrated trajectory. Functionally, this interaction is crucial for protease activity [5]. However, a difference in the frequency of hydrogen bonds was observed with the other active site residues. The frequency of interaction between atom N1 of DRV and the backbone oxygen of Asp30′ decreased by ~10% in L38HL. Subsequently, a decrease in frequency was witnessed between the backbone nitrogen of Asp29 and O28 of DRV. Further, the interaction between O28 and Asp30 was hindered in L38HL. The reduced frequency of interactions in L38HL may be attributed to the increased flexibility and alterations in the overall shape and compactness of L38HL, which is evident from the radius of gyration and SASA analyses.

3.7 | Binding Free Energy Analyses

To understand the effect of double insertion on the HIV-1 subtype C PR, binding energies of DRV to WT and L38HL were computed using MM/GBSA. The binding free energies of WT and L38HL were found to be −22.06 and −21.168 kcal/mol, respectively. The lower binding free energy indicates the weaker binding of DRV to the L38HL PR variant. This could be due to the reduced frequency of hydrogen bond interactions between the DRV and L38HL resulting from two atomic pairs; namely, Asp30′—DRV N1 and DRV O28—Asp30. These changes may contribute to a less stable binding interface, leading to a lower binding free energy. Further exploration of the dynamic behavior of hinge residues could yield valuable insights into the mechanistic disparities in the binding of DRV between the WT and the L38HL PR variant.

To facilitate a comparison with other drugs, docking calculations were carried out for 10 FDA-approved HIV PIs. Table 3 presents the docking scores for 10 drugs docked against the HIV protease WT subtype C. The docking score for DRV was −6.72 kcal/mol. Saquinavir (SQV) and Indinavir (IDV) showed higher docking scores relative to the other drugs, indicating enhanced interactions. Conversely, Ritonavir (RTV) showed the lowest docking score at −5.33 kcal/mol.

3.8 | Effect of Insertion on the Dynamics of Leu38 Backbone

Structural changes can occur at both global and local levels due to variations in the protein. All the above-performed analyses underscore the global structural changes in the L38HL structures. To effectively assess the impact of the double insertion on the backbone sampling, the dihedral angles at the site of insertion, Leu38/Leu38′, were explicitly analyzed. Figure 6 displays the histogram distribution of Φ and Ψ angles corresponding to Leu38. In the WT, the Φ values for both chain A and chain B are distributed between −160° and −50°, indicating a similar sampling of Φ angles in both chains (Figure 6A). However, notable differences were observed between chain A and chain B for L38HL. A single peak distribution of Φ angle between −80° and −40° in L38HL chain A suggests restricted sampling, whereas a much broader distribution (between −180° and −40°) was observed for chain B (Figure 6B).

TABLE 1 | Hydrogen bond interactions observed between WT and DRV during the simulation, along with their frequency of occurrence.

Acceptor		Donor		
Residue name	Atom	Residue name	Atom	Frequency
Asp 25′	OD2	DRV	O18	0.99
DRV	O18	Asp 25	OD2	0.92
Asp 30′	O	DRV	N1	0.76
DRV	O28	Asp 29	N	0.47
DRV	O28	Asp 30	N	0.13

TABLE 2 | Hydrogen bond interactions observed between L38HL and DRV during the simulation, along with their frequency of occurrence.

Acceptor		Donor		
Residue name	Atom	Residue name	Atom	Frequency
Asp 25′	OD2	DRV	O18	0.99
DRV	O18	Asp 25	OD2	0.95
Asp 30′	O	DRV	N1	0.67
DRV	O28	Asp 29	N	0.42

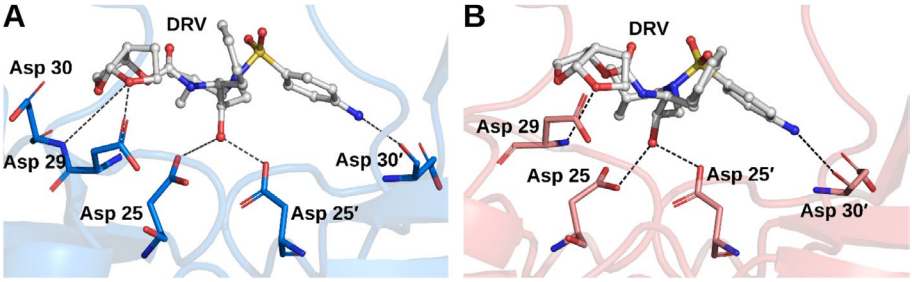

FIGURE 5 | Representative conformations of hydrogen bond interactions in (A) WT and (B) L38HL. DRV is shown in ball-and-stick representation, and the interacting residues are represented in sticks. The hydrogen bonds between atoms of the binding site residues and those of DRV are indicated by dashed lines.

TABLE 3 | Docking scores of 10 FDA-approved drugs.

Drugs	Docking score (kcal/mol)
Darunavir (DRV)	−6.72
Atazanavir (ATV)	−6.63
Amprenavir (APV)	−5.71
Saquinavir (SQV)	−8.36
Fosamprenavir (FPV)	−5.57
Indinavir (IDV)	−8.11
Ritonavir (RTV)	−5.33
Tipranavir (TPV)	−7.00
Nelfinavir (NFV)	−7.50
Lopinavir (LPV)	−6.22

Also, chain B exhibited a distribution similar to the WT, with considerable overlapping regions. Overall, in both WT and L38HL, chain B exhibited a consistent distribution of Φ angles, with significant overlap (Figure 6B). However, there was a notable disparity in the sampling of Φ angles in chain A between the two (Figure 6A).

Similar to Φ angles, the WT displayed a similar distribution in chains A and B for the Ψ angles (Figure 6C). A comparison of the WT chain A Ψ distribution with L38HL revealed a shift in the peak (Figure 6C). Interestingly, no overlaps were observed, indicating a completely different sampling of Ψ angles. In L38HL Chain A, the angles were in the range of −80° to 100° and 100° to 150° for WT. A similar trend was observed in the Ψ angles of L38HL chain B (25–170). However, the distribution showed two peaks (at 50° and 150°), with the second peak having a partial overlap with the WT distribution (Figure 6D).

3.9 | Examining the Conformational Changes in DRV due to Insertion

The ligand RMSD showed a significant difference between the L38HL and WT PR structures. The insertion induced a noticeable change in the protease's shape, affecting its binding to DRV. In Figure 7A, the RMSD shift between WT and L38HL is illustrated. The time evolution of RMSD for WT and L38HL is given in SI Figure S3. The change in RMSD was calculated by subtracting the RMSD value of WT from that of L38HL. A positive change in RMSD indicates an increase in RMSD of DRV in L38HL relative to the WT. Based on the RMSD analysis of the L38HL protease, significant changes in the protease structure in the R1–R3 region were observed. A distinct shift in the R3 structure may have resulted from the twisting of the R2 region (Figure 7B), which could be attributed to reduced hydrogen bonding with DRV in L38HL. These structural changes have impacted the dynamics of the ligand, leading to a decrease in hydrogen bonds between L38HL and DRV and, consequently, a diminished binding affinity.

4 | Discussion

HIV protease serves as a crucial target in combating AIDS. The selection pressure, together with the dynamic nature of viral replication, has led to different subtypes of HIV [5]. The PR subtype, which is most prevalent in the sub-Saharan and African regions, is the HIV-PR subtype C [4]. Further, an insertion variant of subtype C has been reported [17]. However, the existing FDA-approved drugs are designed for targeting subtype B. Hence, this study focuses on effectively understanding the PR ligand interactions between second-generation FDA-approved drug DRV and the relatively less explored HIV PR subtype C using molecular dynamics simulations.

HIV PR functions in a concerted fashion. Thus, the overall dynamics of the enzyme are critical for its effective functioning. However, the insertion in L38HL has led to significant perturbations in the structural dynamics, as evidenced by the change in RMSD (Figure 2A,B). Further comparison of the representative conformations from WT and L38HL revealed an RMSD of ~0.7 Å caused by substantial structural changes at the hinge and fulcrum regions. Nevertheless, the change in RMSD could also lead to effective binding of the drugs. Thus, RMSF analysis was performed to examine the impact of such structural changes at the functionally important regions such as the hinge and the fulcrum on the overall structural flexibility [34]. While the core catalytic residues maintain stability, increased fluctuations were observed for residues at the insertion site. Moreover, the fluctuations at the site of insertion were more in chain B than in chain A, indicating that, despite being a homodimer, the insertion has a different impact on both the chains.

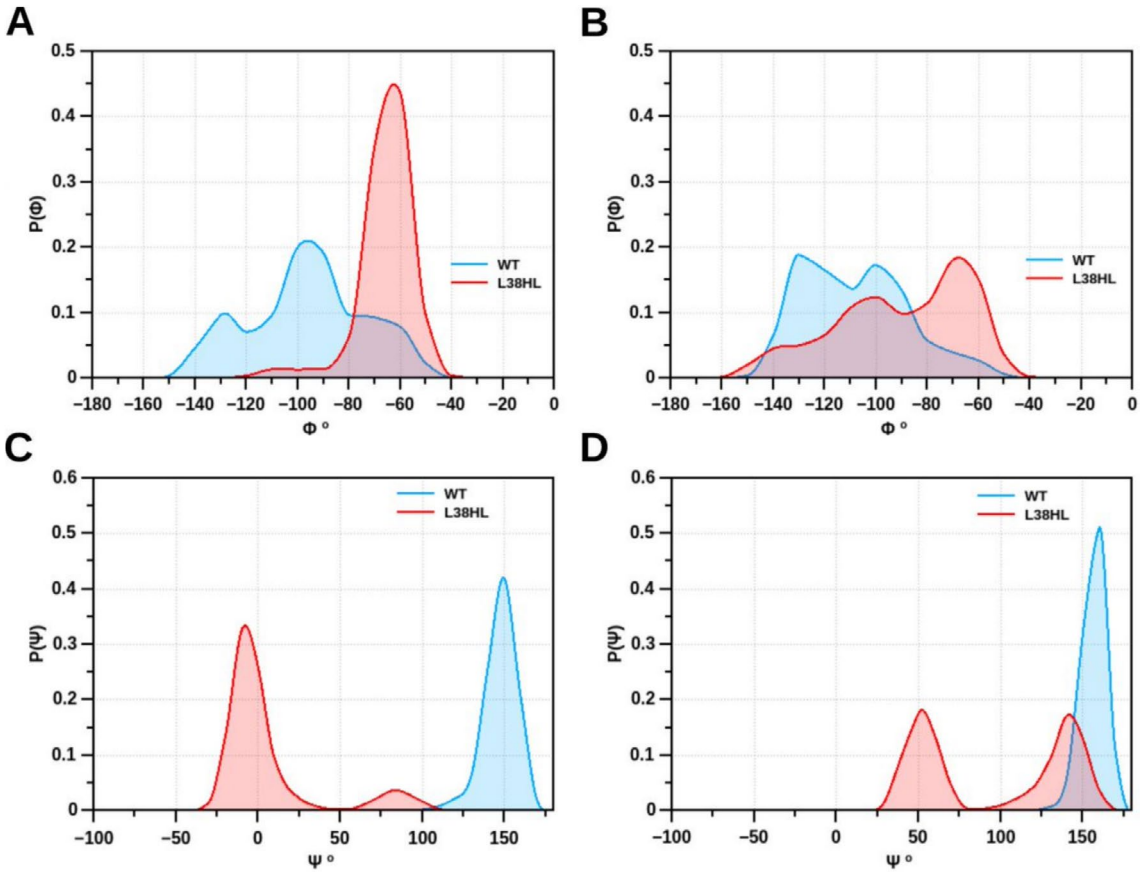

FIGURE 6 | Normalized distributions of Φ angles (A) chain A, (B) chain B, and Ψ angles (C) chain A, (D) chain B corresponding to WT and L38HL.

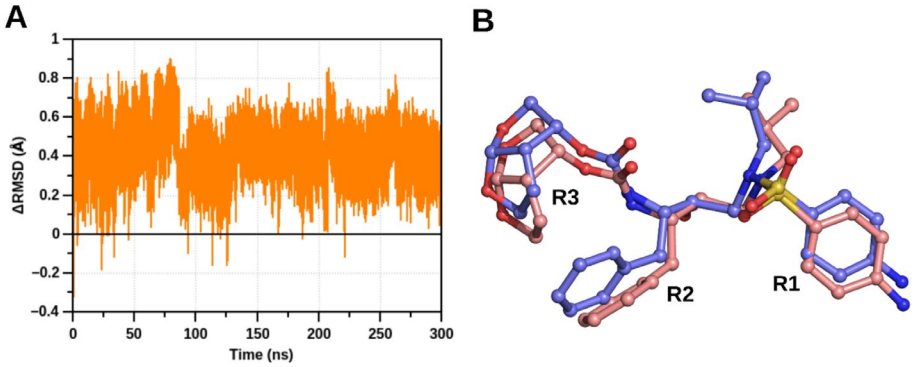

FIGURE 7 | (A) Change in ligand RMSD between WT and L38HL (excluding hydrogens). (B) Representative structures of DRV highlighting the conformational differences between WT (blue) and L38HL (pink).

A plausible explanation for the increase in fluctuations at the hinge may stem from the Φ and Ψ angles. These increased fluctuations could perturb the overall dynamics [34], leading to a loss of compactness which is witnessed by the proportionate increase in SASA and R_g for the L38HL variant (Figure 3C,D). This further supports the notion that the insertion at the hinge profoundly impacts the overall PR dynamics. The observed increase in SASA and R_g for L38HL could be attributed to the loss in hydrophobic compactness, which may in turn influence the drug binding landscape of L38HL [35]. These changes in HIV PR have been suggested to be one of the mechanisms by which the secondary mutations (mutations away from the active site) induce drug resistance [5]. These results agree with our prior study on HIV PR subtype C, which delved into the structural effects of L38HL insertion when bound to SQV [36].

Dynamic cross-correlation analyses revealed a shift in the direction of movement of residues at the insertion site. Specifically, a positive correlation between the flap residues in L38HL (absent in WT) suggests that in L38HL, the directionality of atomic coordinate fluctuation of these residues is the same. The RMSF and cross-correlation results distinctly indicate that insertion impacts the internal dynamics of the protease. Further, the alteration impacts the directionality of motion and the correlated movement of residues at the flap and hinge regions [37].

Previous studies have demonstrated that intrinsic changes in HIV may alter the molecular interactions leading to drug resistance [38]. Analysis of the hydrogen bond interactions between the PR and DRV indicates the loss of interactions in L38HL between Asp30 and DRV. The loss of interactions can be attributed to the conformational changes that occur in L38HL and DRV (Figure 7B). These changes consequently result in lower binding energy in L38HL, leading to drug resistance. The results from the docking analyses align with our previous study [39], in which the binding free energy of ATV was found to be −12.91 kcal/mol, which is significantly lower than that of DRV. These results emphasize the necessity of focusing drug development specific to subtype C.

Based on our simulation study, it was observed that the insertion of residues at the hinge induces variations in Φ and Ψ angles. These variations lead to increased residue fluctuations at the hinge, resulting in increased SASA and R_g of the PR structure. The alterations in overall structure compactness signify changes in the hydrophobic core, which is crucial for drug binding. Given that the functioning of PR relies on coordinated movements of flaps, hinge, fucrum and cantilever, subtle structural changes also lead to the loss of hydrogen bond interactions, ultimately reducing the binding energy between L38HL and DRV, thereby causing drug resistance.

5 | Conclusions

The molecular dynamics study on HIV PR subtype C WT and L38HL bound to DRV shed light on the change in drug susceptibility due to secondary mutations. We investigated the structural changes and intermolecular interactions of both proteases to assess the potential emergence of drug resistance caused by insertion. Notably, the L38HL variant showed heightened flexibility in the hinge resembling drug-resistant mutations documented in previous studies. Furthermore, the results from binding free energy values revealed that the L38HL insertion reduced the protease's affinity for DRV. The subtle change in the binding affinity arises from the loss of hydrogen bond interactions, which in turn was affected by the change in the overall compactness and increased residue level fluctuations caused by altered dihedral angles due to the insertion. These findings provide insights into the potential development of a drug for HIV PR subtype C.

Author Contributions

Sankaran Venkatachalam: methodology, data curation, formal analysis, validation, investigation, writing – original draft, writing – review and editing. **Sowmya Ramaswamy Krishnan:** investigation, methodology, formal analysis, writing – review and editing. **Ramesh Pandian:** methodology, data curation, formal analysis, writing – review and editing. **Yasien Sayed:** conceptualization, methodology, supervision, project administration, funding acquisition, writing – review and editing. **M. Michael Gromiha:** conceptualization, methodology, validation, supervision, funding acquisition, project administration, resources, writing – review and editing.

Acknowledgments

We thank the Department of Biotechnology and Indian Institute of Technology Madras for computational facilities. The work is partially supported by the Department of Science and Technology, Government of India under the BRICS project (DST/ICD/BRICS/Call-3/HIV protease/2019) to M.M.G., and the South African National Research Foundation (NRF) via the BRICS multilateral joint science and technology research collaboration (Grant number: 120452) to Y.S.

Data Availability Statement

The data that support the findings of this study are available from the corresponding author upon reasonable request.

Peer Review

The peer review history for this article is available at https://www.webofscience.com/api/gateway/wos/peer-review/10.1002/prot.26817.

References

1. F. Barré-Sinoussi, J. C. Chermann, F. Rey, et al., "Isolation of a T-Lymphotropic Retrovirus From a Patient at Risk for Acquired Immune Deficiency Syndrome (AIDS)," *Science* 220, no. 4599 (1983): 868–871.

2. R. C. Gallo, P. S. Sarin, E. P. Gelmann, et al., "Isolation of Human T-Cell Leukemia Virus in Acquired Immune Deficiency Syndrome (AIDS)," *Science* 220, no. 4599 (1983): 865–867.

3. World Health Organization, *HIV/AIDS Fact Sheet* (World Health Organization, 2022), Available online https://www.who.int/news-room/fact-sheets/detail/hiv-aids.

4. L. Dwyer-Lindgren, M. A. Cork, A. Sligar, et al., "Mapping HIV Prevalence in Sub-Saharan Africa Between 2000 and 2017," *Nature* 570, no. 7760 (2019): 189–193.

5. I. T. Weber, Y. F. Wang, and R. W. Harrison, "HIV Protease: Historical Perspective and Current Research," *Viruses* 13, no. 5 (2021): 839.

6. L. Buonaguro, M. L. Tornesello, and F. M. Buonaguro, "Human Immunodeficiency Virus Type 1 Subtype Distribution in the Worldwide Epidemic: Pathogenetic and Therapeutic Implications," *Journal of Virology* 81, no. 19 (2007): 10209–10219.

7. D. S. Clutter, M. R. Jordan, S. Bertagnolio, and R. W. Shafer, "HIV-1 Drug Resistance and Resistance Testing," *Infection, Genetics and Evolution* 46 (2016): 292–307.

8. S. B. Lloyd, S. J. Kent, and W. R. Winnall, "The High Cost of Fidelity," *AIDS Research and Human Retroviruses* 30, no. 1 (2014): 8–16.

9. R. P. Smyth, M. P. Davenport, and J. Mak, "The Origin of Genetic Diversity in HIV-1," *Virus Research* 169, no. 2 (2012): 415–429.

10. R. Gupta, A. Hill, A. W. Sawyer, and D. Pillay, "Emergence of Drug Resistance in HIV Type 1-Infected Patients After Receipt of First-Line Highly Active Antiretroviral Therapy: A Systematic Review of Clinical Trials," *Clinical Infectious Diseases* 47, no. 5 (2008): 712–722.

11. S. Sierra and H. Walter, "Targets for Inhibition of HIV Replication: Entry, Enzyme Action, Release and Maturation," *Intervirology* 55, no. 2 (2012): 84–97.

12. M. A. Navia, P. M. Fitzgerald, B. M. McKeever, et al., "Three-Dimensional Structure of Aspartyl Protease From Human Immunodeficiency Virus HIV-1," *Nature* 337, no. 6208 (1989): 615–620.

13. B. R. Meher and S. Patel, "Structural and Dynamical Aspects of HIV-1 Protease and its Role in Drug Resistance," *Advances in Protein Chemistry and Structural Biology* 92 (2013): 299–324.

14. A. K. Ghosh, H. L. Osswald, and G. Prato, "Recent Progress in the Development of HIV-1 Protease Inhibitors for the Treatment of HIV/AIDS," *Journal of Medicinal Chemistry* 59, no. 11 (2016): 5172–5208.

15. A. M. Wensing, N. M. van Maarseveen, and M. Nijhuis, "Fifteen Years of HIV Protease Inhibitors: Raising the Barrier to Resistance," *Antiviral Research* 85, no. 1 (2010): 59–74.

16. P. Naicker, I. Achilonu, S. Fanucchi, et al., "Structural Insights Into the South African HIV-1 Subtype C Protease: Impact of Hinge Region Dynamics and Flap Flexibility in Drug Resistance," *Journal of Biomolecular Structure and Dynamics* 31, no. 12 (2013): 1370–1380.

17. J. Ledwaba, Y. Sayed, V. Pillay, L. Morris, and G. Hunt, "Low Frequency of Protease Inhibitor Resistance Mutations and Insertions in HIV-1 Subtype C Protease Inhibitor-Naive Sequences," *AIDS Research and Human Retroviruses* 35, no. 7 (2019): 673–678.

18. S. Mosebi, L. Morris, H. W. Dirr, and Y. Sayed, "Active-Site Mutations in the South African Human Immunodeficiency Virus Type 1 Subtype C Protease Have a Significant Impact on Clinical Inhibitor Binding: Kinetic and Thermodynamic Study," *Journal of Virology* 82, no. 22 (2008): 11476–11479.

19. R. W. Shafer, T. K. Chuang, P. Hsu, C. B. White, and D. A. Katzenstein, "Sequence and Drug Susceptibility of Subtype C Protease From Human Immunodeficiency Virus Type 1 Seroconverters in Zimbabwe," *AIDS Research and Human Retroviruses* 15, no. 1 (1999): 65–69.

20. A. K. Ghosh, Z. L. Dawson, and H. Mitsuya, "Darunavir, a Conceptually New HIV-1 Protease Inhibitor for the Treatment of Drug-Resistant HIV," *Bioorganic & Medicinal Chemistry* 15, no. 24 (2007): 7576–7580.

21. Y. Shabanpour, S. Sajjadi, E. Behmard, P. Abdolmaleki, and A. H. Keihan, "The Structural, Dynamic, and Thermodynamic Basis of Darunavir Resistance of a Heavily Mutated HIV-1 Protease Using Molecular Dynamics Simulation," *Frontiers in Molecular Biosciences* 9 (2022): 927373.

22. B. Webb and A. Sali, "Comparative Protein Structure Modeling Using MODELLER," *Current Protocols in Bioinformatics* 54, no. 1 (2016): 5–6.

23. S. Jo, T. Kim, V. G. Iyer, and W. Im, "CHARMM-GUI: A Web-Based Graphical User Interface for CHARMM," *Journal of Computational Chemistry* 29, no. 11 (2008): 1859–1865.

24. J. A. Maier, C. Martinez, K. Kasavajhala, L. Wickstrom, K. E. Hauser, and C. Simmerling, "ff14SB: Improving the Accuracy of Protein Side Chain and Backbone Parameters From ff99SB," *Journal of Chemical Theory and Computation* 11, no. 8 (2015): 3696–3713.

25. J. Wang, R. M. Wolf, J. W. Caldwell, P. A. Kollman, and D. A. Case, "Development and Testing of a General Amber Force Field," *Journal of Computational Chemistry* 25, no. 9 (2004): 1157–1174.

26. D. A. Case, H. M. Aktulga, K. Belfon, et al., "AmberTools," *Journal of Chemical Information and Modeling* 63, no. 20 (2023): 6183–6191.

27. T. Darden, D. York, and L. Pedersen, "Particle Mesh Ewald: An N·Log (N) Method for Ewald Sums in Large Systems," *Journal of Chemical Physics* 98, no. 12 (1993): 10089–10092.

28. J. P. Ryckaert, G. Ciccotti, and H. J. Berendsen, "Numerical Integration of the Cartesian Equations of Motion of a System With Constraints: Molecular Dynamics of n-Alkanes," *Journal of Computational Physics* 23, no. 3 (1977): 327–341.

29. T. S. Lee, D. S. Cerutti, D. Mermelstein, et al., "GPU-Accelerated Molecular Dynamics and Free Energy Methods in Amber18: Performance Enhancements and New Features," *Journal of Chemical Information and Modeling* 58, no. 10 (2018): 2043–2050.

30. P. A. Kollman, I. Massova, C. Reyes, et al., "Calculating Structures and Free Energies of Complex Molecules: Combining Molecular Mechanics and Continuum Models," *Accounts of Chemical Research* 33, no. 12 (2000): 889–897.

31. V. Tsui and D. A. Case, "Theory and Applications of the Generalized Born Solvation Model in Macromolecular Simulations," *Biopolymers* 56, no. 4 (2000): 275–291.

32. M. Karplus and J. N. Kushick, "Method for Estimating the Configurational Entropy of Macromolecules," *Macromolecules* 14, no. 2 (1981): 325–332.

33. C. Okamoto and K. Ando, "Molecular Dynamics Simulation Analysis of Structural Dynamic Cross Correlation Induced by Odorant Hydrogen-Bonding in Mouse Eugenol Ol-Factory Receptor," *Biophysics and Physicobiology* 21, no. 1 (2024): e210007.

34. D. Sherry, R. Worth, Z. S. Ismail, and Y. Sayed, "Cantilever-Centric Mechanism of Cooperative Non-active Site Mutations in HIV Protease: Implications for Flap Dynamics," *Journal of Molecular Graphics and Modelling* 106 (2021): 107931.

35. S. Mittal, Y. Cai, M. N. Nalam, D. N. Bolon, and C. A. Schiffer, "Hydrophobic Core Flexibility Modulates Enzyme Activity in HIV-1 Protease," *Journal of the American Chemical Society* 134, no. 9 (2012): 4163–4168.

36. S. Venkatachalam, N. Murlidharan, S. R. Krishnan, et al., "Understanding Drug Resistance of Wild-Type and L38HL Insertion Mutant of HIV-1 C Protease to Saquinavir," *Genes* 14, no. 2 (2023): 533.

37. R. G. Wang, H. X. Zhang, and Q. C. Zheng, "Revealing the Binding and Drug Resistance Mechanism of Amprenavir, Indinavir, Ritonavir, and Nelfinavir Complexed With HIV-1 Protease due to Double Mutations G48T/L89M by Molecular Dynamics Simulations and Free Energy Analyses," *Physical Chemistry Chemical Physics* 22, no. 8 (2020): 4464–4480.

38. Y. Yu, J. Wang, Q. Shao, J. Shi, and W. Zhu, "Effects of Drug-Resistant Mutations on the Dynamic Properties of HIV-1 Protease and Inhibition by Amprenavir and Darunavir," *Scientific Reports* 5, no. 1 (2015): 10517.

39. S. V. Sankaran, S. R. Krishnan, Y. Sayed, and M. M. Gromiha, "Mechanism of Drug Resistance in HIV-1 Protease Subtype C in the Presence of Atazanavir," *Current Research in Structural Biology* 7 (2024): 100132.

Supporting Information

Additional supporting information can be found online in the Supporting Information section.